

Screening-induced temperature-dependent transport in two-dimensional graphene

E. H. Hwang and S. Das Sarma

Condensed Matter Theory Center, Department of Physics, University of Maryland, College Park, Maryland 20742-4111, USA

(Received 7 November 2008; revised manuscript received 12 March 2009; published 6 April 2009)

We calculate the temperature-dependent conductivity of graphene in the presence of randomly distributed Coulomb impurity charges arising from the temperature-dependent screening of the Coulomb disorder without any phonons. The purely electronic temperature dependence of our theory arises from two independent mechanisms: the explicit temperature dependence of the finite-temperature dielectric function $\epsilon(q, T)$ and the finite-temperature energy averaging of the transport scattering time. We find that the calculated temperature-dependent conductivity is nonmonotonic, decreasing with temperature at low temperatures, and increasing at high temperatures. We provide a critical comparison with the corresponding physics in semiconductor-based parabolic band 2D electron-gas systems.

DOI: [10.1103/PhysRevB.79.165404](https://doi.org/10.1103/PhysRevB.79.165404)

PACS number(s): 81.05.Uw, 72.10.-d, 72.15.Lh, 72.20.Dp

I. INTRODUCTION

Ever since the successful fabrication of gated two-dimensional (2D) graphene monolayers and the measurement of the density-dependent (i.e., gate voltage tuned) conductivity of 2D chiral graphene carriers,¹ transport properties of 2D graphene layers have been of great interest to both experimentalists¹⁻¹⁰ and theorists.¹¹⁻¹⁵ Much of the early interest focused on the important issue of the scattering mechanisms limiting the low-temperature conductivity and the associated graphene “minimal conductivity” at the charge neutral (Dirac) point. One of the dominant low-temperature scattering mechanisms^{3,4,13-15} in graphene is that due to screened Coulomb scattering by unintended charged impurities invariably present in the graphene environment, e.g., the substrate (and the substrate-graphene interface). By reducing the concentration of charged impurities in suspended graphene,^{6,10} very high quality samples (with mobilities exceeding 200 000 cm²/Vs which is an order of magnitude improvement over graphene samples fabricated on a substrate) have been made.

There has been substantial recent experimental⁷⁻¹⁰ and theoretical¹¹⁻²⁰ work on both density and temperature dependence of graphene carrier transport properties. Much of the observed temperature-dependent graphene properties have been theoretically studied in the context of the phonon-scattering mechanism¹⁶⁻²⁰ which freezes out at low temperatures. Our theoretical work presented in the current paper considers temperature-dependent graphene transport arising entirely out of electronic mechanisms without any phonon effects. Our motivation is partially theoretical, but we are also motivated by the intriguing recent experimental observation⁷⁻¹⁰ of an increasing graphene conductivity with increasing temperature at the Dirac point, which obviously cannot be explained by phonons since phonon scattering necessarily leads to an increasing carrier resistivity with increasing temperature (as is seen in graphene at higher carrier densities away from the Dirac point).

Our theoretical motivation for studying temperature-dependent graphene transport associated with purely electronic mechanisms arises from the extensively studied 2D metal-insulator-transition phenomena^{21,22} in semiconductor-

based 2D systems. The low-temperature resistivity measurements in conventional semiconductor-based 2D systems (e.g., Si inversion layers, GaAs heterostructures, and quantum wells) report the observation of an anomalously strong temperature dependent (showing an effective metallic behavior) 2D conductivity.^{21,22} In conventional 2D structures long-range charged impurity scattering dominates low-temperature Ohmic transport and it is known that the temperature-dependent screening of charged impurity scattering gives rise to the unusual strong temperature-dependent metallic behavior at low carrier densities.²³ Since in gated graphene layers, which are similar to 2D electron systems in confined semiconductor structures, the charged impurities are also the main scattering mechanism, one can expect a strong temperature-dependent conductivity. However, a very weak (less than 5%) temperature-dependent conductivity from 1 K to room temperature has been reported for low mobility graphene samples.¹

Recently, with more careful measurements in high mobility samples a strong temperature dependence of carrier conductivity is reported.⁷⁻¹⁰ We first summarize the key experimental features of the measured carrier transport in 2D high mobility graphene sample. Experimentally one finds a density (n^*) separating an effective metallic behavior (for density $n > n^*$) from an effective insulating behavior ($n < n^*$),¹⁰ where metal insulator is defined by whether $d\rho/dT > 0$ or < 0 . The effective metallic behavior is characterized by a drop in the temperature-dependent resistivity, $\rho(T)$, as $T \rightarrow 0$. At low density, near the charge neutral Dirac point, the conductivity of graphene shows a pronounced nonmetallic T dependence (i.e., the increase of resistivity with decreasing T). In this paper, we propose a possible theoretical explanation for (at least a part of) the observed temperature-dependent conductivity in graphene at low carrier density. We emphasize that the apparent insulating behavior near the Dirac point cannot be explained by phonons. Our explanation is quantitative, microscopic, and physically motivated. Our theory is based on an essential assumption, that is, transport is dominated by charged impurity-scattering centers (with a density of n_i per unit area) which are randomly distributed in the graphene environment. We use the finite-temperature Drude-Boltzmann theory to calculate the Ohmic resistivity of the graphene electrons.^{23,24} We calculate the

graphene conductivity in the presence of randomly distributed Coulomb impurity charges near the surface with the electron-impurity interaction being screened by the 2D graphene carriers in the random phase approximation (RPA). The screened Coulomb scattering is the only scattering mechanism in our theory. We also compare critically the 2D graphene situation with the corresponding situation in the conventional parabolic 2D electron-gas systems.

We neglect all phonon-scattering effects in this calculation, which have been considered recently finding that acoustic phonon scattering gives rise to a linear resistivity with temperature.^{16,17} Given that 2D graphene is essentially a weakly interacting system with effective $r_s \sim 0.88$ for graphene on SiO₂, which is defined by the ratio of the potential energy to the kinetic energy, $r_s = P.E/K.E = e^2/\kappa\hbar v_F$, and the effective fine structure constant independent of carrier density, we expect our RPA-Boltzmann theory to be a quantitatively and qualitatively accurate description of graphene transport for all practical purposes.

The paper is organized as follows. In Sec. II the Boltzmann transport theory is presented to calculate temperature-dependent 2D graphene conductivity. In Sec. III we study the temperature-dependent screening function. Section IV presents the results of the calculations. We conclude in Sec. V with a discussion.

II. CONDUCTIVITY IN BOLTZMANN THEORY

The low-energy band Hamiltonian for graphene is well approximated by a two-dimensional Dirac equation for massless particles, the so-called Dirac-Weyl equation,²⁵

$$H = \hbar v_F (\sigma_x k_x + \sigma_y k_y), \quad (1)$$

where v_F is the 2D Fermi velocity, σ_x and σ_y are Pauli spinors, and \mathbf{k} is the momentum relative to the Dirac points. The corresponding eigenstates are given by the plane wave,

$$\psi_{s\mathbf{k}}(\mathbf{r}) = \frac{1}{\sqrt{A}} \exp(i\mathbf{k} \cdot \mathbf{r}) F_{s\mathbf{k}}, \quad (2)$$

where A is the area of the system, $s = \pm 1$ indicate the conduction (+1) and valence (-1) bands, respectively, and $F_{s\mathbf{k}}^\dagger = \frac{1}{\sqrt{2}}(e^{i\theta_{\mathbf{k}}}, s)$ with $\theta_{\mathbf{k}} = \tan(k_y/k_x)$ being the polar angle of the momentum \mathbf{k} . The corresponding energy of graphene for 2D wave vector \mathbf{k} is given by $\epsilon_{s\mathbf{k}} = s v_F |\mathbf{k}|$, and the density of states (DOS) is given by $D(\epsilon) = g |\epsilon| / (2\pi\hbar^2 v_F^2)$, where $g = g_s g_v$ is the total degeneracy ($g_s = 2$, $g_v = 2$ being the spin and valley degeneracies, respectively).

When the external field is weak and the displacement of the distribution function from the thermal equilibrium is small, we may write the distribution function to the lowest order in the applied electric field (\mathbf{E}) $f_{s\mathbf{k}} = f(\epsilon_{s\mathbf{k}}) + g_{s\mathbf{k}}$, where $f(\epsilon_{s\mathbf{k}})$ is the equilibrium Fermi distribution function and $g_{s\mathbf{k}}$ is proportional to the field. Assuming spatial uniformity and the steady state electric field, the Boltzmann transport equation is written as

$$\begin{aligned} \left(\frac{df_{s\mathbf{k}}}{dt} \right)_c &= \frac{d\mathbf{k}}{dt} \cdot \frac{\partial f(\epsilon_{s\mathbf{k}})}{\partial \mathbf{k}} = -e\mathbf{E} \cdot \mathbf{v}_{s\mathbf{k}} \frac{\partial f}{\partial \epsilon_{s\mathbf{k}}} \\ &= - \int \frac{d^2 k'}{(2\pi)^2} (g_{s\mathbf{k}} - g_{s\mathbf{k}'}) W_{s\mathbf{k},s'\mathbf{k}'}, \end{aligned} \quad (3)$$

where $v_{s\mathbf{k}} = s v_F \mathbf{k} / |\mathbf{k}|$ is the electron velocity, and $W_{s\mathbf{k},s'\mathbf{k}'}$ is the quantum mechanical scattering probability. Within the Born approximation $W_{s\mathbf{k},s'\mathbf{k}'}$ for scattering from $s'\mathbf{k}'$ to $s\mathbf{k}$ can be written by

$$W_{s\mathbf{k},s'\mathbf{k}'} = \frac{2\pi}{\hbar} n_i |\langle V_{s\mathbf{k},s'\mathbf{k}'} \rangle|^2 \delta(\epsilon_{s\mathbf{k}} - \epsilon_{s'\mathbf{k}'}), \quad (4)$$

where $\langle V_{s\mathbf{k},s'\mathbf{k}'} \rangle$ is the matrix element of the scattering potential associated with impurity disorder in the graphene environment, and n_i the number of impurities per unit area. Following the usual approximation scheme we have assumed an ensemble averaging over random uncorrelated impurities. Note that since we consider elastic impurity scattering, the interband processes ($s \neq s'$) are not permitted. When the relaxation-time approximation is valid, we have

$$g_{s\mathbf{k}} = - \frac{\tau(\epsilon_{s\mathbf{k}})}{\hbar} e\mathbf{E} \cdot \mathbf{v}_{s\mathbf{k}} \frac{\partial f(\epsilon_{s\mathbf{k}})}{\partial \epsilon_{s\mathbf{k}}}, \quad (5)$$

where $\tau(\epsilon_{s\mathbf{k}})$ is the relaxation time or the transport scattering time,²⁶ and is given by

$$\frac{1}{\tau(\epsilon_{s\mathbf{k}})} = \frac{2\pi n_i}{\hbar} \int \frac{d^2 k'}{(2\pi)^2} |\langle V_{s\mathbf{k},s'\mathbf{k}'} \rangle|^2 [1 - \cos \theta_{\mathbf{k}\mathbf{k}'}] \delta(\epsilon_{s\mathbf{k}} - \epsilon_{s'\mathbf{k}'}), \quad (6)$$

where $\theta_{\mathbf{k}\mathbf{k}'}$ is the scattering angle between the scattering in- and out-wave vectors \mathbf{k} and \mathbf{k}' .

The electrical current density is given by

$$\mathbf{j} = g \int \frac{d^2 k}{(2\pi)^2} e \mathbf{v}_{s\mathbf{k}} f_{s\mathbf{k}}. \quad (7)$$

Using Eq. (5) we obtain the conductivity in Boltzmann transport theory by averaging over energy,

$$\sigma = \frac{e^2 v_F^2}{2} \int d\epsilon D(\epsilon) \tau(\epsilon) \left(- \frac{\partial f}{\partial \epsilon} \right), \quad (8)$$

and the corresponding temperature-dependent resistivity is given by $\rho(T) = 1/\sigma(T)$. Note that $f(\epsilon_k)$ is the Fermi distribution function, $f(\epsilon_k) = \{1 + \exp[(\epsilon_k - \mu)/k_B T]\}^{-1}$ where the finite-temperature chemical potential, $\mu(T)$, is determined self-consistently to conserve the total number of electrons. At $T=0$, $f(\epsilon)$ is a step function at the Fermi energy $E_F \equiv \mu(T=0)$, and we then recover the usual conductivity formula: $\sigma = \frac{e^2 v_F^2}{2} D(E_F) \tau(E_F)$.

The matrix element of the scattering potential of randomly distributed screened impurity charge centers in graphene is given by

$$|\langle V_{\mathbf{s}\mathbf{k},\mathbf{s}\mathbf{k}'} \rangle|^2 = \left| \frac{v_i(q)}{\varepsilon(q)} \right|^2 \frac{1 + \cos \theta}{2}, \quad (9)$$

where $q = |\mathbf{k} - \mathbf{k}'|$, $\theta \equiv \theta_{\mathbf{k}\mathbf{k}'}$, and $v_i(q) = 2\pi e^2 / (\kappa q)$ is the Fourier transform of the 2D Coulomb potential in an effective background lattice dielectric constant κ . The factor $(1 + \cos \theta)/2$ arises from the sublattice symmetry (overlap of wave function).¹¹ In Eq. (9), $\varepsilon(q) \equiv \varepsilon(q, T)$ is the 2D finite-temperature static RPA dielectric (screening) function appropriate for graphene,²⁷ given by $\varepsilon(q, T) = 1 + v_c(q)\Pi(q, T)$, where $\Pi(q, T)$ is the graphene irreducible finite-temperature polarizability function and $v_c(q)$ is the Coulomb interaction. Then, the energy dependent scattering time $\tau(\epsilon_k)$ for our model is given in the leading-order theory by

$$\frac{1}{\tau(\epsilon_k)} = \frac{\pi n_i}{\hbar} \int \frac{d^2 k'}{(2\pi)^2} \left| \frac{v_i(q)}{\varepsilon(q, T)} \right|^2 \delta(\epsilon_{\mathbf{k}} - \epsilon_{\mathbf{k}'}) \times (1 - \cos \theta)(1 + \cos \theta). \quad (10)$$

The factor $(1 - \cos \theta)$ in Eq. (10) weights the amount of backward scattering of the electron by the impurity. The $(1 - \cos \theta)$ factor, associated with the vertex correction by impurity interaction in the diagrammatic calculation of the conductivity, is always present in transport theories involving elastic scattering. In normal parabolic 2D systems the factor $(1 - \cos \theta)$ obviously favors large-angle scattering events, in particular, the $+k_F$ to $-k_F$ backward scattering. However, in graphene the large-angle scattering is also suppressed due to the wave function overlap factor $(1 + \cos \theta)$, which arises from the sublattice symmetry peculiar to graphene. The energy dependent scattering time in graphene thus gets weighted by an angular contribution factor of $(1 - \cos \theta) \times (1 + \cos \theta)$, which suppresses both small-angle scattering and large-angle scattering contributions in the scattering rate. Therefore, τ is insensitive to both small- and large-angle scatterings. In fact, the dominant contribution to τ comes from $\cos^2 \theta = 0$, i.e., $\theta = \pi/2$ scattering, which is equivalent to the k_F “right-angle” scattering in contrast to the $2k_F$ back scattering in ordinary 2D systems. The importance of the right-angle scattering in 2D graphene has not been emphasized in the literature.

We note that there are two independent sources of temperature-dependent resistivity in our calculation. One comes from the energy averaging defined in Eq. (8), and the other is the explicit temperature dependence of the finite-temperature dielectric function $\varepsilon(q, T)$ which produces a direct temperature dependence through screening in Eq. (10), i.e., $\tau(\epsilon)$ in Eq. (10) also depends explicitly on T due to the dependence of $\varepsilon(q, T)$ on T . Even if τ does not have any explicit T dependence the finite-temperature energy averaging of Eq. (8) by itself introduces a temperature dependence as long as $\tau(\epsilon)$ has some energy dependence. For example, if the relaxation time $\tau(\epsilon)$ is given by a function of energy ϵ as $\tau \propto \epsilon^\alpha$, then we have $\sigma \propto T^{1+\alpha}$. We describe the details of energy dependent scattering time and temperature-dependent scattering time in Secs. III and IV.

Before concluding this basic transport theory section of this paper we want to point out the key qualitative similarities and differences in the transport theory between 2D

graphene and 2D semiconductor-based parabolic 2D systems (e.g., Si MOSFETs, GaAs heterostructures and quantum wells, SiGe-based 2D structures) which have been studied extensively over the last 30 years.^{22,24} First, the formal Boltzmann theory for carrier transport is the same in both systems except for the different angular factor, $(1 - \cos \theta)$ in the conventional 2D systems and $(1 - \cos^2 \theta)$ in Eq. (10) for 2D graphene. Formally the two theories become identical for isotropic s -wave disorder, where the scattering potential is zero range (i.e., a constant in the wave vector space).²⁶ But for the long-range Coulomb disorder associated with scattering by random charged impurities in the environment, which is of interest in this work, the factor $(1 - \cos \theta)$ and $(1 - \cos^2 \theta)$ in Eq. (10) would have very different implications.²⁶ Of course, the explicit differences between 2D graphene and 2D parabolic systems in the density of states $D(\epsilon)$ in Eq. (8) and the dielectric function $\varepsilon(q, T)$ in Eq. (10) would lead to different temperature-dependent conductivities in these two systems even if the angular factors were the same.

The importance of k_F scattering in graphene versus $2k_F$ scattering in the ordinary 2D semiconductor systems in determining the transport properties, most particularly the temperature-dependent conductivity, cannot be overemphasized. For example, theoretical approaches to understanding the temperature-dependent graphene conductivity using the impurity-induced Friedel oscillations^{12,28} (i.e., the $2k_F$ behavior of the polarizability function) immediately run into problem, as mentioned above, because unlike the regular 2D systems, k_F scattering, not the $2k_F$ scattering, dominates graphene transport. In fact, while both approaches lead to the prediction of weak temperature-dependent conductivity in graphene at low temperatures in contrast to regular 2D system, the $2k_F$ Friedel oscillation approach predicts¹² a weak insulating temperature dependence for high-density extrinsic 2D graphene whereas the k_F approach based on the screening theory used in the current work leads to a weak metallic graphene conductivity at low T/T_F . This is a qualitative and conceptual difference, which applies whenever screening is important in determining graphene transport properties.

III. TEMPERATURE-DEPENDENT POLARIZABILITY AND SCREENING

The important temperature dependence of the scattering time τ arises from the temperature-dependent screening in Eq. (10). Thus, before we discuss the temperature-dependent conductivity we first consider temperature-dependent screening (or dielectric function) i.e.,

$$\epsilon(q, T) = 1 + v_c \Pi(q, T), \quad (11)$$

where $\Pi(q, T)$ is the graphene irreducible finite-temperature polarizability function, which is given by the bare bubble diagram (calculated at $T=0$ in Ref. 27 for 2D graphene)

$$\Pi(q, T) = - \frac{g}{A} \sum_{\mathbf{k}, \mathbf{s}\mathbf{k}'} \frac{f_{\mathbf{s}\mathbf{k}} - f_{\mathbf{s}'\mathbf{k}'}}{\epsilon_{\mathbf{s}\mathbf{k}} - \epsilon_{\mathbf{s}'\mathbf{k}'}} F_{ss'}(\mathbf{k}, \mathbf{k}'), \quad (12)$$

where $\mathbf{k}' = \mathbf{k} + \mathbf{q}$, $\epsilon_{\mathbf{s}\mathbf{k}} = s\hbar v_F |\mathbf{k}|$, and $f_{\mathbf{s}\mathbf{k}} = [\exp\{\beta(\epsilon_{\mathbf{s}\mathbf{k}} - \mu)\} + 1]^{-1}$, where the finite-temperature chemical potential $\mu(T)$

is determined by the conservation of the total electron density as

$$\frac{1}{2} \left(\frac{T_F}{T} \right)^2 = F_1(\beta\mu) - F_1(-\beta\mu), \quad (13)$$

where $\beta = 1/k_B T$ and $F_n(x)$ is given by

$$F_n(x) = \int_0^\infty \frac{t^n dt}{1 + \exp(t-x)}. \quad (14)$$

The limiting forms of the function $F_1(x)$ are given by

$$F_1(x) \approx \frac{\pi^2}{12} + x \ln 2 + \frac{x^2}{4} \quad \text{for } |x| \ll 1, \quad (15)$$

$$F_1(x) \approx \left[\frac{x^2}{2} + \frac{\pi^2}{6} \right] \theta(x) + x \ln(1 + e^{-|x|}) \quad \text{for } |x| \gg 1. \quad (16)$$

Thus we have the chemical potential in both low- and high-temperature limits for graphene as

$$\mu(T) \approx E_F \left[1 - \frac{\pi^2}{6} \left(\frac{T}{T_F} \right)^2 \right] \quad \text{for } T/T_F \ll 1, \quad (17)$$

$$\mu(T) \approx \frac{E_F}{4 \ln 2} \frac{T_F}{T} \quad \text{for } T/T_F \gg 1. \quad (18)$$

After performing the summation over ss' one can rewrite the polarizability as

$$\Pi(q, T) = \Pi^+(q, T) + \Pi^-(q, T), \quad (19)$$

where

$$\begin{aligned} \Pi^+(q, T) = & -\frac{g}{2L^2} \sum_k \left[\frac{[f_{\mathbf{k}+} - f_{\mathbf{k}'+}](1 + \cos \theta_{kk'})}{\epsilon_{\mathbf{k}} - \epsilon_{\mathbf{k}'}} \right. \\ & \left. + \frac{[f_{\mathbf{k}+} + f_{\mathbf{k}'+}](1 - \cos \theta_{kk'})}{\epsilon_{\mathbf{k}} + \epsilon_{\mathbf{k}'}} \right], \quad (20) \end{aligned}$$

and

$$\begin{aligned} \Pi^-(q, T) = & -\frac{g}{2L^2} \sum_k \left[-\frac{[f_{\mathbf{k}-} - f_{\mathbf{k}'-}](1 + \cos \theta_{kk'})}{\epsilon_{\mathbf{k}} - \epsilon_{\mathbf{k}'}} \right. \\ & \left. - \frac{[f_{\mathbf{k}-} + f_{\mathbf{k}'-}](1 - \cos \theta_{kk'})}{\epsilon_{\mathbf{k}} + \epsilon_{\mathbf{k}'}} \right], \quad (21) \end{aligned}$$

where $\epsilon_{\mathbf{k}} = \hbar v_F |\mathbf{k}|$, and $\cos \theta_{kk'} = (k+q \cos \phi) / |\mathbf{k} + \mathbf{q}|$, and ϕ is an angle between \mathbf{k} and \mathbf{q} . After performing angular integration and using the dimensionless quantities $\tilde{\Pi} = \Pi/D_0$, where $D_0 \equiv gE_F/2\pi\hbar^2 v_F^2$ is the DOS at Fermi level, we have

$$\begin{aligned} \tilde{\Pi}^+(q, T) = & \frac{\mu}{E_F} + \frac{T}{T_F} \ln(1 + e^{-\beta\mu}) \\ & - \frac{1}{k_F} \int_0^{q/2} dk \frac{\sqrt{1 - (2k/q)^2}}{1 + \exp[\beta(\epsilon_k - \mu)]}, \quad (22) \end{aligned}$$

and

$$\begin{aligned} \tilde{\Pi}^-(q, T) = & \frac{\pi q}{8 k_F} + \frac{T}{T_F} \ln(1 + e^{-\beta\mu}) \\ & - \frac{1}{k_F} \int_0^{q/2} dk \frac{\sqrt{1 - (2k/q)^2}}{1 + \exp[\beta(\epsilon_k + \mu)]}. \quad (23) \end{aligned}$$

At $T=0$, $\mu(T=0)=E_F$ and Eqs. (22) and (23) become the zero temperature polarizabilities, i.e.,

$$\tilde{\Pi}^+(q) = \begin{cases} 1 - \frac{\pi q}{8k_F}, & q \leq 2k_F \\ 1 - \frac{1}{2} \sqrt{1 - \frac{4k_F^2}{q^2}} - \frac{q}{4k_F} \sin^{-1} \frac{2k_F}{q}, & q > 2k_F, \end{cases} \quad (24)$$

and

$$\tilde{\Pi}^-(q) = \frac{\pi q}{8k_F}. \quad (25)$$

From Eqs. (22) and (23) we have the asymptotic form of polarizability at high temperatures ($T \gg T_F$),

$$\tilde{\Pi}(q, T) \approx \frac{T}{T_F} \ln 4 + \frac{q^2}{24k_F^2} \frac{T_F}{T}, \quad (26)$$

and at low temperatures ($T \ll T_F$),

$$\tilde{\Pi}(q, T) \approx \frac{\mu(T)}{E_F} = 1 - \frac{\pi^2}{6} \left(\frac{T}{T_F} \right)^2 \quad \text{for } \epsilon_q < 2\mu,$$

$$\begin{aligned} \tilde{\Pi}(q, T) \approx & \frac{\mu}{E_F} \left[1 - \frac{1}{2} \sqrt{1 - \left(\frac{2\mu}{\epsilon_q} \right)^2} - \frac{\epsilon_q}{2\mu} \sin^{-1} \frac{2\mu}{\epsilon_q} \right] \\ & + \frac{\pi q}{8k_F} + \frac{2\pi^2 T^2 E_F \mu}{3 T_F^2 \epsilon_q^2} \\ & \times \frac{1}{\sqrt{1 - (2\mu/\epsilon_q)^2}} \quad \text{for } \epsilon_q > 2\mu. \quad (27) \end{aligned}$$

For $q=2k_F$ we then have

$$\tilde{\Pi}(q=2k_F, T) \approx \frac{\mu(T)}{E_F} + \sqrt{\frac{\pi\mu}{2E_F}} \left[1 - \frac{\sqrt{2}}{2} \right] \zeta\left(\frac{3}{2}\right) \left(\frac{T}{T_F} \right)^{3/2}, \quad (28)$$

where $\zeta(x)$ is Riemann's zeta function.

To obtain the screening constant or the screening wave vector q_s , we note that the screened potential,

$$U(q) = \frac{v(q)}{\epsilon(q)} = \frac{2\pi e^2}{\kappa q [1 + v_c \Pi(q)]} = \frac{2\pi e^2}{\kappa(q + q_s)}, \quad (29)$$

so that, $q_s(q) = q v_c(q) \Pi(q) = 2\pi e^2 \Pi(q) / \kappa$. In the $q \rightarrow 0$ long wavelength limit, we then have the finite-temperature Thomas-Fermi wave vector as

$$q_s(T) \approx 8 \ln(2) r_s k_F \left(\frac{T}{T_F} \right) \quad \text{for } T \gg T_F,$$

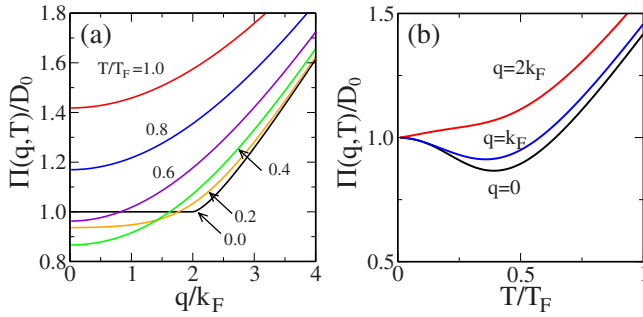


FIG. 1. (Color online) Temperature-dependent graphene polarizability (a) as a function of wave vector for different temperatures and (b) as a function of temperature for different wave vectors.

$$\approx 4r_s k_F \left[1 - \frac{\pi^2}{6} \left(\frac{T}{T_F} \right)^2 \right] \quad \text{for } T \ll T_F. \quad (30)$$

The screening wave vector increases linearly with temperature at high temperatures ($T \gg T_F$), but becomes a constant with a small quadratic correction at low temperatures ($T \ll T_F$).

In Fig. 1 we show the finite-temperature polarizability $\Pi(q, T)$ (a) for different temperatures as a function of wave vector, and (b) for different wave vectors as a function of temperature. Note that for $q < 2k_F$ the total polarizability has a local minimum near $T \approx 0.45T_F$, however it increases monotonically for $q \geq 2k_F$, which arises from the excitation of electrons from the valence band to the conduction band. The different temperature dependence between small wave vectors ($q < 2k_F$) and large wave vectors ($q > 2k_F$) gives rise to very different temperature-dependent scattering rates for 2D graphene, Eq. (10), compared to that of ordinary 2D systems. In graphene the chiral sublattice symmetry suppresses backward (i.e., a scattering induced wave vector change by $2k_F$ from $+k_F$ to $-k_F$) scattering, so the temperature dependence of screening at $q = 2k_F$ is not significant for conductivity while the temperature dependence of screening at large-angle scattering ($2k_F$) always dominates the temperature-dependent conductivity in ordinary 2D systems. In graphene we have to consider the temperature dependence of polarizability at $q \sim k_F$ rather than at $q = 2k_F$ in order to understand temperature-dependent conductivity due to the screening because k_F (rather than $2k_F$) scattering dominates graphene transport properties. Since the graphene polarizability at $2k_F$ increases monotonically with temperature, the temperature dependence of resistivity caused by $2k_F$ scattering (or equivalently the thermal suppression of the Friedel oscillation—the behavior of polarizability at $q = 2k_F$ is closely related to Friedel oscillations) decreases with increasing temperature. Recently¹² the Friedel oscillation was considered in graphene and a linear temperature-dependent correction to the graphene resistivity was obtained based purely on the $2k_F$ scattering in analogy with the corresponding parabolic 2D systems. However, as we mentioned above, this correction to the resistivity arising from the $2k_F$ scattering is negative in graphene in contrast to the regular 2D systems (i.e., insulating behavior, or the resistivity decreases as temperature increases), which disagrees with the experimental

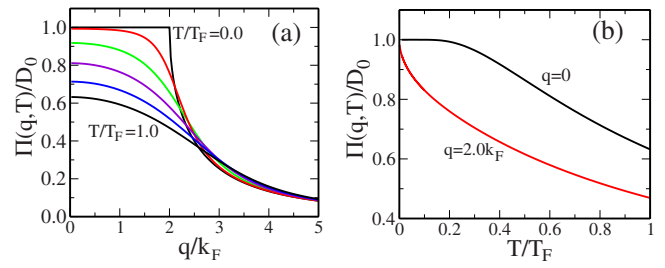


FIG. 2. (Color online) (a) The 2D polarizability function $\Pi(q, T)/D_0$, which is normalized to the density of states at Fermi level ($D_0 = gm/\hbar^2 \pi$), as a function of dimensionless wave vector q/k_F , where k_F is the Fermi wave vector, for several different temperatures $T/T_F = 0, 0.2, 0.4, 0.6, 0.8, 1.0$ (top to bottom). In (b) $\Pi(q, T)/D_0$ is shown as a function of temperature for different wave vectors. The strong temperature-induced suppression of the $2k_F$ Kohn anomaly in screening is evident in the figure even for very low T/T_F . A comparison with Fig. 1 shows the compelling qualitative difference between graphene screening and ordinary 2D screening behaviors.

observation. In graphene, since the most dominant scattering happens at $q \sim k_F$ we have to investigate the temperature-dependent polarizability at $q \sim k_F$, which decreases with temperature (for $T \ll T_F$) and gives rise to the increases in resistivity with temperature as observed experimentally.

Now we compare the temperature-dependent polarizability of graphene with that of ordinary 2D systems. In Fig. 2 we show the corresponding parabolic 2D polarizability normalized by the density of states at Fermi level, $D_0 = gm/\hbar^2 2\pi$, where g is a degeneracy factor and m is the effective mass of electron. Note that the temperature dependence of 2D polarizability at $q = 2k_F$ is much stronger than that of graphene polarizability. Since in normal 2D systems the $2k_F$ scattering event is most important for the electrical resistivity, the temperature dependence of polarizability at $q = 2k_F$ completely dominates at low temperatures ($T \ll T_F$). It is known that the strong temperature dependence of the polarizability function at $q = 2k_F$ (see Fig. 2) leads to the anomalously strong temperature-dependent resistivity in ordinary 2D systems.²³ However, the relatively weak temperature dependence of graphene polarizability for $q \sim k_F$ compared with the 2D polarizability function at $q = 2k_F$ should lead to a weak temperature-dependent resistivity in graphene for $T \ll T_F$.

Finally, an analytic comparison between graphene and 2D parabolic systems completes the comparison between 2D graphene and 2D parabolic semiconductor screening properties, as shown in Figs. 1 and 2, respectively. We provide below the low ($T \ll T_F$) and the high ($T \gg T_F$) temperature analytic limits for the regular 2D polarizability function in both the $q = 0$ Thomas-Fermi and the $q = 2k_F$ Friedel oscillation regimes [to be contrasted with the corresponding graphene formula given in Eqs. (26)–(28) above]. For $T \ll T_F$

$$\Pi_{2D}(q = 0, T) \approx D_{2D} [1 - e^{-T_F/T}], \quad (31)$$

$$\Pi_{2D}(2k_F, T) \approx D_{2D} \left[1 - \sqrt{\frac{\pi}{4}} (1 - \sqrt{2}) \zeta\left(\frac{1}{2}\right) \sqrt{\frac{T}{T_F}} \right], \quad (32)$$

and for $T \gg T_F$

$$\Pi_{2D}(q, T) \approx D_{2D} \frac{T_F}{T} \left[1 - \frac{q^2 T_F}{6k_F^2 T} \right], \quad (33)$$

where $D_{2D} = gm/2\pi\hbar^2$ is the regular 2D DOS. We note that in the $T \gg T_F$ limit, the Fermi surface is completely thermally suppressed, and therefore the $2k_F$ screening or $2k_F$ -Friedel oscillation does not carry any special significance, leading to the same $T \gg T_F$ asymptotic screening formula in Eq. (33) for all wave vectors. For $q=0$, in the $T \gg T_F$ limit, we get the usual Debye screening for the regular 2D electron-gas system, which follows from putting $q=0$ in Eq. (33),

$$\Pi_{2D}(q=0, T \gg T_F) \approx D_{2D} \frac{T_F}{T}. \quad (34)$$

For graphene the corresponding high-temperature screening formula can be easily derived to be

$$\Pi(q, T \gg T_F) \approx D_0 \frac{T}{T_F} \left[\ln 4 + \frac{q^2}{24k_F^2} \left(\frac{T_F}{T}\right)^2 \right]. \quad (35)$$

A comparison of Eqs. (34) and (35) shows that the high-temperature Debye screening behavior is different in graphene and regular 2D systems just as the low-temperature screening behaviors also are.

In Sec. IV we calculate the temperature-dependent graphene conductivity due to the scattering by screened Coulomb impurities using the temperature-dependent screening properties calculated in this section.

IV. CONDUCTIVITY RESULTS

A. $\sigma(T)$ due to screening

Using the temperature-dependent screening wave vector, $q_s(T)$ of Eq. (30), we can calculate analytically the temperature-dependent scattering time of charged Coulomb impurities arising purely from screening in systematic $T/T_F \ll 1$ or $\gg 1$ asymptotic expansions in the low- and high-temperature limits,

$$\begin{aligned} \frac{1}{\tau(T)} &= \frac{n_i}{2\pi\hbar} \frac{\varepsilon_k}{(\hbar v_F)^2} \int_0^\pi d\theta (1 - \cos^2 \theta) \frac{v_i(q)^2}{\varepsilon(q, T)^2} \\ &= \frac{n_i}{2\pi\hbar} \left(\frac{2\pi e^2}{\kappa}\right)^2 \frac{2}{\varepsilon_k} \int_0^1 dx \frac{x^2 \sqrt{1-x^2}}{[x + q_s(T)/2k]^2}. \end{aligned} \quad (36)$$

At low temperatures ($T \ll T_F$) we have

$$\frac{1}{\tau(T)} \approx \frac{1}{\tau_0} \left[1 + \frac{2\pi^2 r_s I_1}{3 I_0} \left(\frac{T}{T_F}\right)^2 \right], \quad (37)$$

where $\tau_0 = \tau(T=0)$ is the scattering time at $T=0$ and given by²⁶

$$\frac{1}{\tau_0} = \frac{n_i}{2\pi\hbar} \left(\frac{2\pi e^2}{\kappa}\right)^2 \frac{2I_0}{E_F}, \quad (38)$$

and

$$I_n = \int_0^1 dx \frac{x^2 \sqrt{1-x^2}}{(x+2r_s)^{2+n}} = -\frac{2}{1+n} \frac{\partial I_{n-1}}{\partial r_s}. \quad (39)$$

At high temperatures ($T \gg T_F$) we have

$$\frac{1}{\tau(T)} \approx \frac{1}{\tau_0} \frac{\pi}{16I_0} \left(\frac{1}{4 \ln(2)r_s}\right)^2 \left(\frac{T_F}{T}\right)^2. \quad (40)$$

Then from Eq. (8) with $T=T_F$ we have the temperature-dependent conductivity due to screening at low temperatures ($T \ll T_F$),

$$\frac{\sigma(T)}{\sigma_0} \approx 1 - \frac{2\pi^2 r_s I_1}{3 I_0} \left(\frac{T}{T_F}\right)^2, \quad (41)$$

where $\sigma_0 = e^2 v_F^2 D(E_F) \tau_0 / 2$. The calculated conductivity decreases quadratically as the temperature increases and shows typical metallic temperature dependence. On the other hand, at high temperatures ($T/T_F \gg 1$) we have

$$\frac{\sigma(T)}{\sigma_0} \approx \frac{16I_0}{\pi} [4 \ln(2)r_s]^2 \left(\frac{T}{T_F}\right)^2. \quad (42)$$

The temperature-dependent conductivity due to screening effects increases as the temperature increases in the high-temperature regime, characteristic of an insulating system. We note that the temperature dependence is weak for $T \ll T_F$ and is strong for $T \gg T_F$.

B. $\sigma(T)$ due to energy averaging

Let us now discuss the temperature-dependent conductivity due to energy averaging. For graphene the energy dependent scattering time can be expressed by

$$\frac{1}{\tau(\varepsilon)} = \frac{n_i}{2\pi\hbar} \frac{\varepsilon_k}{(\hbar v_F)^2} \int_0^{2k} \frac{dq q^2}{k^2} \sqrt{1 - \left(\frac{q}{2k}\right)^2} \frac{v_i(q)^2}{\varepsilon(q, T)^2}, \quad (43)$$

where $\varepsilon_k = \hbar v_F k$ and $v_i(q)$ the impurity-scattering potential. For the unscreened Coulomb potential $\varepsilon(q, T) = 1$ and $v_i(q) = 2\pi e^2 / \kappa q$. Thus we have

$$\frac{1}{\tau(\varepsilon)} = \frac{1}{\tau_1} \frac{E_F}{\varepsilon_k}, \quad (44)$$

where

$$\frac{1}{\tau_1} = \frac{n_i}{4\hbar} \left(\frac{2\pi e^2}{\kappa}\right)^2 \frac{1}{E_F}. \quad (45)$$

Then from Eq. (8) we have

$$\sigma(T) = \frac{\sigma_1}{E_F^2} \int_0^\infty d\varepsilon \varepsilon^2 \left(-\frac{\partial f}{\partial \varepsilon}\right) = \sigma_1 \frac{2T^2}{T_F} F_1(\beta\mu), \quad (46)$$

where $\sigma_1 = e^2 v_F^2 D(E_F) \tau_1 / 2$. Using Eqs. (15) and (16) we have the conductivities for the unscreened Coulomb potential scattering in the low-temperature limit ($T \ll T_F$),

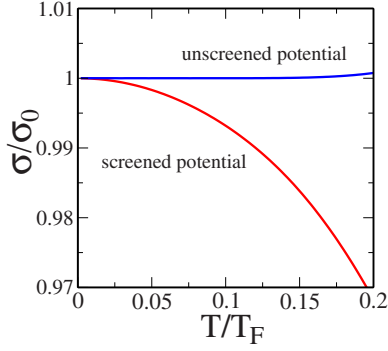


FIG. 3. (Color online) Temperature-dependent conductivity for unscreened Coulomb potential (top line) and screened potential (bottom line) in the low-temperature limit.

$$\sigma(T) \approx \sigma_1 \left[\left(\frac{\mu}{E_F} \right)^2 + \frac{\pi^2}{3} \left(\frac{T}{T_F} \right)^2 \right] \approx \sigma_1 \{ 1 + O[(T/T_F)^4] \}, \quad (47)$$

and in the high-temperature limit ($T \gg T_F$),

$$\sigma(T) \approx \sigma_1 \frac{\pi^2}{6} \left(\frac{T}{T_F} \right)^2. \quad (48)$$

Therefore the temperature-dependent conductivity, as implied by energy averaging only, is almost a constant in the low-temperature limit (see the top line in Fig. 3). But at high temperatures the conductivity due to energy averaging increases as T^2 similar to screening effects.

Now consider the screened Coulomb potential scattering. Expanding Eq. (43) with respect to $(\varepsilon - E_F)$ we have

$$\frac{1}{\tau(\varepsilon)} \approx \frac{1}{\tau_0} \frac{\varepsilon_k}{E_F} \left[1 - a_1 \frac{\varepsilon_k - E_F}{E_F} + a_2 \frac{(\varepsilon_k - E_F)^2}{E_F^2} \right], \quad (49)$$

where $a_1 = 2J_1/J_0$, $a_2 = 3J_2/J_0$, where

$$J_n = \int_0^1 dx \frac{x^{2+n} \sqrt{1-x^2}}{(x+q_0)^{2+n}}, \quad (50)$$

where $q_0 = q_{TF}/2k_F = 2r_s$. Then from Eq. (8) we have

$$\begin{aligned} \frac{\sigma(T)}{\sigma_0} &\approx \int_0^\infty d\varepsilon \left(-\frac{\partial f}{\partial \varepsilon} \right) \\ &\times \left[1 + a_1 \frac{\varepsilon - E_F}{E_F} + (a_1^2 - a_2) \frac{(\varepsilon - E_F)^2}{E_F^2} \right] \approx 1 \\ &- \frac{\pi^2}{3} \left(\frac{a_1}{2} - a_1^2 + a_2 \right) \left(\frac{T}{T_F} \right)^2. \end{aligned} \quad (51)$$

With $r_s = 0.88$ we have $a_1 = 0.52$ and $a_2 = 0.22$. Therefore, the temperature-dependent conductivity due to energy averaging becomes

$$\sigma(T) = \sigma_0 \left[1 - \frac{\pi^2}{3} 0.21 \left(\frac{T}{T_F} \right)^2 \right]. \quad (52)$$

For screened Coulomb potential the conductivity shows metallic behavior, again the temperature-dependent correction

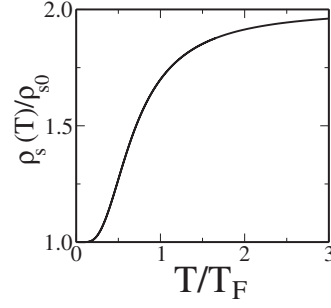


FIG. 4. Calculated resistivity arising from the short-range white-noise disorder scattering as a function of scaled temperature T/T_F . Here $\rho_s(T) = 1/\sigma_s(T)$ and $\rho_{s0} = 1/\sigma_s(T=0)$.

being quadratically weak in the small parameter $t \equiv T/T_F \ll 1$. Combining results from Secs. IV A and IV B, we conclude that the $T/T_F \ll 1$ graphene conductivity will have weak quadratic metallic corrections, and for $T \gg T_F$ the conductivity increases proportional to $(T/T_F)^2$.

Finally in this section, we comment briefly on the temperature dependence of the conductivity arising from the short-range white-noise disorder scattering, which may be important in graphene (as well as regular 2D parabolic electron systems in semiconductor heterostructures) at high carrier densities, where Coulomb disorder effects are typically screened out. The temperature dependence of conductivity for both graphene and regular 2D systems due to unscreened short-range disorder arises now entirely from the energy averaging effect by definition since the short-range disorder is considered unscreened. It is easy to calculate $\sigma_s(T)$ of graphene due to the short-range disorder (with scattering strength $v_i = v_0$) by carrying out the appropriate energy averaging, we have

$$\sigma_s(T) = \frac{\sigma_{s0}}{1 + e^{-\beta\mu}}, \quad (53)$$

where $\sigma_{s0} = e^2 v_F^2 D(E_F) \tau_s / 2$ with $\tau_s = \frac{n_i}{4\hbar} E_F v_0^2 / (\hbar v_F)^2$. The following analytic asymptotic results are obtained:

$$\sigma(T \ll T_F) \approx \sigma_{s0} [1 - e^{-T_F/T}], \quad (54)$$

$$\sigma(T \gg T_F) \approx \frac{\sigma_{s0}}{2} \left[1 + \frac{1}{8 \ln 2} \left(\frac{T_F}{T} \right)^2 \right]. \quad (55)$$

In the low-temperature limit the temperature dependence of conductivity is exponentially suppressed, but the high-temperature limit of the conductivity approaches $\sigma_{s0}/2$ as $T \rightarrow \infty$, i.e., the resistivity at high temperatures increases up to a factor of 2 compared with the low-temperature limit resistivity. In Fig. 4 we show the calculated resistivity due to the short-range disorder scattering.

For the sake of completeness, we provide below the equations describing the asymptotic low²⁹ and high³⁰ temperature behaviors of 2D conductivity for the usual gaped parabolic 2D electron system as found in Si MOSFETs and GaAs heterostructures,

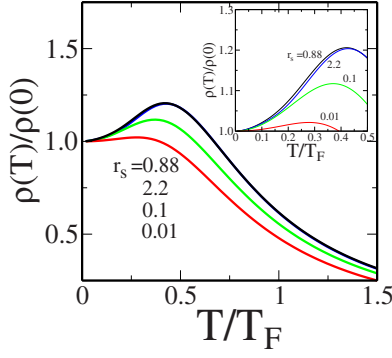


FIG. 5. (Color online) Calculated resistivity as a function of scaled temperature T/T_F for different $r_s=0.88, 2.2, 0.1, 0.01$ (from top to bottom). $r_s=0.88$ (2.2) corresponds to graphene on the SiO_2 substrate (in vacuum). Inset shows the magnified view in the low-temperature limit $T < 0.5T_F$.

$$\sigma(T \ll T_F) \approx \sigma_0^{2D} \left[1 - C_1 \left(\frac{T}{T_F} \right) - C_2 \left(\frac{T}{T_F} \right)^{2/3} \right], \quad (56)$$

$$\sigma(T \gg T_F) \approx \sigma_1^{2D} \left[\frac{T}{T_F} + \frac{3\sqrt{\pi}q_0}{4} \sqrt{\frac{T_F}{T}} \right]. \quad (57)$$

In Eq. (56), $\sigma_0^{2D} \equiv \sigma(T=0)$, and $C_1 = 2q_0/(1+q_0)$, $C_2 = 2.65q_0^2/(1+q_0)^2$, where $q_0 = q_{TF}/2k_F$ (q_{TF} and k_F are the 2D Thomas-Fermi wave vector and Fermi wave vector, respectively). In Eq. (57), $\sigma_1^{2D} = (e^2/h)(n/n_i)\pi q_0^2$. We note that in the parabolic 2D system $q_{TF} = g_s g_v / a_B$, where a_B is the Bohr radius. We have assumed an ideal 2D electron gas here with zero thickness in order to compare with the 2D graphene sheet which also has a zero thickness.

In comparing graphene temperature dependence with the regular parabolic 2D system, we note the following similarities and differences: (i) For $T \ll T_F$, both graphene and parabolic 2D systems manifest metallic temperature-dependent conductivity; (ii) the low-temperature ($T \ll T_F$) conductivity manifests much stronger linear temperature dependence in the parabolic 2D system compared with the quadratic temperature dependence in graphene; (iii) at high temperatures ($T \gg T_F$), both systems manifest insulating temperature dependence, but with different power laws in temperature.

C. Numerical results

In this section we present our directly numerically calculated resistivities of Eq. (8) incorporating all effects discussed Secs. IV A and IV B. Our numerical results agree completely with the analytic results given in Secs. IV A and IV B of this paper in the appropriate $T/T_F \ll 1$ and $\gg 1$ limits.

In Fig. 5 we show our calculated resistivity as a function of temperature for different r_s values. Here $r_s=0.88$ (2.2) corresponds to graphene on SiO_2 substrate (in vacuum). The small values of r_s , independent of carrier density and representing the fine structure constant of graphene indicate a weak-coupling system in terms of electron-electron interaction. Note that the calculated $\rho(T)/\rho(T=0)$ scales for all electron densities, and therefore results can be shown as a

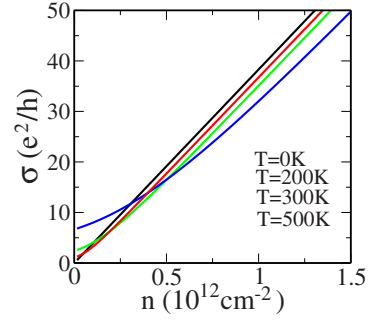


FIG. 6. (Color online) Calculated conductivity for different temperatures $T=0, 200, 300, 500$ K (top to bottom) as a function of density. We use $r_s=0.88$ and an impurity density $n_i=5 \times 10^{11} \text{ cm}^{-2}$.

function of a single dimensionless temperature variable T/T_F for a specific r_s value, i.e., $\rho(T) \equiv \rho(T/T_F; r_s)$. Thus, Fig. 5 can be applied for all graphene samples for a given r_s value. In the low-temperature limit the calculated $\rho(T)$ increases weakly quadratically with temperature, manifesting metallic behavior. But at high temperature $\rho(T)$ decreases quadratically. Thus, we find that the calculated resistivity shows a nonmonotonicity, i.e., at low temperatures the resistivity shows metallic behavior and at high temperatures it shows insulating behavior. The nonmonotonicity of temperature dependent $\rho(T)$ can be understood from the screening behavior: the temperature-dependent polarizability of graphene shows nonmonotonic behavior for $q < 2k_F$. The metallic behavior is the strongest at $r_s \approx 1$, and it becomes weaker as r_s decreases. For $r_s > 1$ the strength of metallic behavior decreases very slowly (see the inset of Fig. 5).

In Fig. 6 we show the calculated temperature-dependent conductivity for different temperatures as a function of density. In the high (low) density limit the conductivity decreases (increases) as the temperature increases. Therefore the conductivity shows a nonmonotonic behavior, i.e., $\sigma(T)$ has a local minimum at a finite temperature.

For comparison we show, in Fig. 7, the calculated temperature-dependent resistivity of ordinary 2D systems for different interaction parameters $r_s (= me^2 / \kappa \sqrt{\pi n})$, which for parabolic 2D systems, in contrast to graphene, depend on

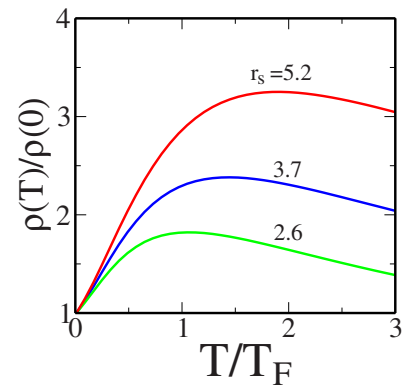


FIG. 7. (Color online) $\rho(T)/\rho(0)$ of an ordinary 2D system for different r_s values as a function of temperature. As r_s increases the metallic behavior becomes stronger.

carrier density. We have used the temperature-dependent polarizability of Fig. 2 in this calculation. Unlike graphene (Fig. 5) the scaled temperature-dependent resistivity of ordinary 2D systems depends strongly on the electron density (or r_s). Since the most dominant scattering occurs at $q=2k_F$ and the temperature dependence of screening function at $2k_F$ is strong, the calculated 2D resistivity shows the strong anomalous linear T metallic behavior, which is observed in many different semiconductor systems [e.g., Si-MOSFET,²¹ p -GaAs,³¹ n -GaAs,³² SiGe,³³ AlAs (Ref. 34)]. In contrast to the ordinary 2D systems the observed resistivity of graphene shows very weak temperature dependence in high-density and low mobility samples.⁷⁻⁹ It has been reported that the measured resistivity change of low mobility high-density samples is less than 10% between 5 and 300 K if one takes out the phonon contribution. The weak temperature dependence of graphene resistivity can be explained by the weak temperature dependence of the screening function. Qualitatively, however, the temperature dependence of graphene resistivity and that of a regular semiconductor-based parabolic 2D system is similar from the perspective of a large change in T/T_F . The calculated $\rho(T)$ for a regular parabolic 2D electron-gas system in the presence of screened Coulomb scattering in the range $T/T_F=0-3$ also shows the nonmonotonicity apparent in Fig. 7, albeit at somewhat higher (r_s -dependent) values of T/T_F . In graphene, see Fig. 5, the resistivity maximum typically occurs around $T/T_F < 0.5$ compared with $T/T_F \sim 1-2$ for parabolic 2D systems as shown in Fig. 7.

Given the great deal of work on the temperature-dependent transport properties of semiconductor-based parabolic 2D electron systems over the last 15 years,²² it may be useful for us to discuss the similarities and differences between these two 2D systems (i.e., graphene and regular 2D electron gas) with respect to the temperature dependence of the resistivity arising from screened Coulomb scattering. The most important qualitative difference is that the leading low-temperature ($T/T_F \ll 1$) correction to the resistivity $\rho(T)$ in ordinary 2D (graphene) systems is linear (quadratic) in temperature—both are metallic corrections, i.e., $\rho(T) \sim \rho_0[1+O(T/T_F)]$ in ordinary 2D systems and $\rho(T) \sim \rho_0[1+O(T/T_F)^2]$ in graphene. This important qualitative difference, of course, leads to a huge quantitative difference between the two systems in the sense that graphene manifests much weaker temperature-dependent resistivity than 2D semiconductor systems at low T/T_F . This difference in the quantitative temperature dependence of the low-temperature resistivity (i.e., linear and strong in 2D systems, and quadratic and weak in graphene) is further exacerbated by the fact that the Fermi temperature in extrinsic graphene tends to be very high (e.g., $T_F \gtrsim 1000$ K for $n \gtrsim 10^{11}$ cm⁻² in graphene) compared with that of semiconductor-based parabolic 2D systems (e.g., $T_F \sim 7$ K for $n \sim 10^{11}$ cm⁻² in Si MOSFETs), leading to much smaller effective values of T/T_F in gated graphene in the extrinsic high-density regime.

The above discussion and the results of Fig. 5 explicitly establish that extrinsic graphene should manifest a very weak screening induced metallic temperature dependence in its low-temperature resistivity. This fact is in qualitative agreement with the available experiments *except* near the Dirac

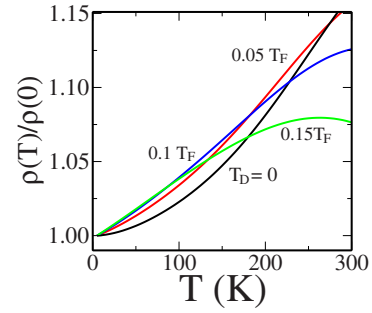


FIG. 8. (Color online) $\rho(T)/\rho(0)$ for $n=5 \times 10^{11}$ cm⁻² and for different Dingle temperatures (level broadening) $T_D=0T_F$, $0.05T_F$, $0.1T_F$, $0.15T_F$ as a function of temperature.

point where the system has very low carrier density (and is almost intrinsic in nature). Taking into account that $T_F(\text{graphene}) \approx 1500\sqrt{\tilde{n}}\text{K}$, where \tilde{n} is the 2D graphene carrier density measured in units of 10^{12} cm⁻², it is obvious that the screening contribution to the temperature-dependent conductivity of graphene, going as $(T/T_F)^2$, would be extremely small in the $T=0-100$ K regime except in the intrinsic regime where $\tilde{n} \ll 1$. The strong metallic temperature dependence of the low-temperature conductivity, which has been much discussed in the context of the 2D metal-insulator transition phenomenon in parabolic 2D semiconductor systems, is therefore absent in gated graphene.

We now discuss the implications of our theory for graphene transport at (or near) the charge neutral Dirac point where the carrier density is very low. Since $\sigma(T/T_F)$ [or $\rho(T/T_F)$] is a universal function of T/T_F in the screening theory, the only difference between the low-density Dirac regime and the high-density extrinsic regime arises from the effective value of T/T_F due to the facts that $T_F \propto \sqrt{n}$, and that the $T/T_F \ll 1$ and $T/T_F \gtrsim 1$ regimes manifest qualitatively different temperature dependence (cf. Fig. 5). For example, for $n \lesssim 10^{10}$ cm⁻², $T_F \lesssim 100$ K, and it is entirely possible for such a low-density regime to manifest the high-temperature “insulating” temperature dependence, as is apparent for $T/T_F \gtrsim 0.5$ in Fig. 5, where $\rho(T)$ decreases with increasing temperature dependence. Close to the Dirac point $T_F (\propto \sqrt{n})$ is arbitrarily small, and therefore the recent experimental observation¹⁰ of a decreasing $\rho(T)$ at low T at the Dirac point may simply be a reflection of this high-temperature insulat-

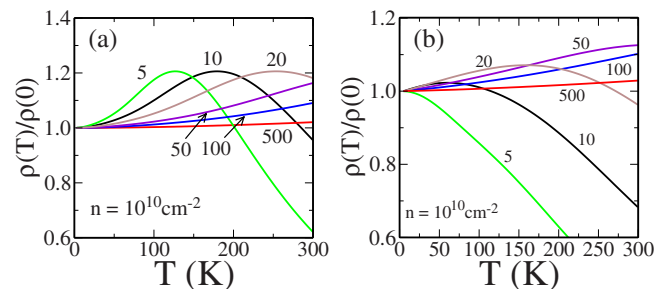


FIG. 9. (Color online) Temperature-dependent resistivity for different densities, $n=5, 10, 20, 50, 100, 500 \times 10^{10}$ cm⁻² as a function of temperature (a) without collisional broadening and (b) with collision broadening of $T_D=100$ K.

TABLE I. Electronic quantities. Note: the carrier effective mass (m) in 2D systems and the graphene Fermi velocity (v_F) are assumed constant independent of carrier density (n) and defining the basic single-particle energy dispersion at wave vector \mathbf{q} : $\varepsilon(\mathbf{q}) = \hbar v_F |\mathbf{q}|$ (graphene) or $\hbar^2 q^2 / 2m$ (2D systems). The degeneracy factor $g = g_s g_v$ carries the usual spin degeneracy ($g_s = 2$) and a valley degeneracy ($g_v = 2$ for graphene).

Quantity	Parabolic 2D system	Graphene
Fermi wave vector (k_F)	$\sqrt{4\pi n/g}$	$\sqrt{4\pi n/g}$
TF screening wave vector (q_{TF})	$gme^2/\kappa\hbar^2$	$ge^2k_F/\kappa\hbar v_F$
Wigner-Seitz radius (r_s)	$me^2/(\kappa\hbar^2\sqrt{\pi n})$	$e^2/\kappa\hbar v_F$
DOS [$D(E)$]	$gm/2\pi\hbar^2$	$gE/(2\pi\hbar^2v_F^2)$
DOS at E_F [$D_0 \equiv D(E_F)$]	$gm/2\pi\hbar^2$	$gk_F/(2\pi\hbar v_F)$
Fermi energy (E_F)	$2\pi n\hbar^2/gm$	$\hbar v_F\sqrt{4\pi n/g}$
Cyclotron frequency (ω_c)	eB/mc	$v_F\sqrt{2e\hbar Bn}$
Landau level energy (E_l)	$(l + \frac{1}{2})\hbar\omega_c \quad l=0, 1, 2, \dots$	$\text{sgn}(l)v_F\sqrt{2e\hbar B l } \quad l=0, \pm 1, \pm 2, \dots$
Plasma frequency [$\omega_p(q)$]	$\sqrt{\frac{2\pi ne^2}{\kappa m}}\sqrt{q}$	$\sqrt{\frac{e^2v_F^4\pi gn}{2\kappa}}\sqrt{q}$

ing behavior arising in our screening theory. The fact that this apparent insulating temperature dependence is observed¹⁰ only at low densities is further evidence in support of the screening scenario.

One puzzling issue in this context is that our theory would predict a metallic $\sigma(T)$ for $T/T_F \ll 1$ independent of carrier density except that the $T/T_F < 1$ regime necessitates going to lower temperatures at lower densities. This seems not to be experimentally observed¹⁰ near the low-density Dirac regime where an insulating temperature dependence is reported at low gate voltage down to the lowest temperatures. One reason for the absence of the metallic regime could be the suppression of the temperature-dependent screening by impurity-scattering induced level broadening as was originally suggested by one of us some time ago.³⁵ Essentially, for $T \lesssim T_D$, where $T_D = \pi\Gamma/k_B$ is the so-called Dingle temperature associated with the impurity-scattering induced level broadening Γ , the temperature dependence of screening is suppressed by scattering effects.^{24,35,36} Such a broadening-induced suppression of the temperature dependence of the screening function $\Pi(q, T)$ for $T \ll T_D$ can be theoretically incorporated in our conductivity calculations, and we discuss below such a scenario. It is clear that this broadening-induced suppression of the temperature dependence of screening will strongly suppress the metallic behavior of the conductivity for $T < T_D$, and may qualitatively explain the experimentally observed insulating $\sigma(T)$ near the Dirac point.¹⁰

In Fig. 8 we show the level broadening effects on $\rho(T)/\rho(0)$. Without level broadening (i.e., $T_D=0$) the low-

temperature metallic behavior of resistivity is quadratic. However, the quadratic temperature dependence is cut off at low temperatures due to the rounding of the sharp corner in the 2D screening function by impurity-scattering effects at very low temperatures $T < T_D$, and the explicit temperature dependence of $\epsilon(q, T)$ is suppressed. Thus, the temperature dependence of graphene resistivity with the level broadening included in the screening function becomes effectively linear at low temperatures.

In Fig. 9 we show the temperature-dependent resistivity for different densities up to room temperature. In the low-density limit the Fermi temperature is low, so we can see both metallic ($T \ll T_F$) and insulating ($T \gtrsim T_F$) behaviors if we neglect collision broadening. However, a finite Dingle temperature suppresses the low-temperature metallic behavior at low densities if $T_D \gtrsim 0.45T_F$, and the system manifests only the insulating $d\rho/dT < 0$ temperature dependence for all temperatures. For high-density samples ($T_D \ll T_F$) we see only the metallic behavior in Fig. 9, and the level broadening gives rise to the linear behavior of the resistivity instead of quadratic behavior at low temperatures. It is possible that this scenario is operational in the experiments of Ref. 10 where an insulating temperature dependence of resistivity is observed in graphene at the low-density intrinsic regime where $T_D \gtrsim T_F$ may apply.

V. CONCLUSION

We have developed a detailed microscopic transport theory for 2D graphene conductivity at finite temperatures,

TABLE II. Temperature-dependent polarizability $\Pi(q, T)$. Note D_0 is DOS at Fermi energy. Here $\zeta(x)$ is Riemann's zeta function.

Temperature (T)	Wave vector (q)	2D Π/D_0	Graphene Π/D_0
Low $T \ll T_F$	$q=0$	$1 - e^{-T_F/T}$	$1 - \frac{\pi^2}{6}(\frac{T}{T_F})^2$
	$q=2k_F$	$1 - \sqrt{\frac{\pi}{4}}(1 - \sqrt{2})\zeta(\frac{1}{2})\sqrt{\frac{T}{T_F}}$	$1 + \sqrt{\frac{\pi}{2}}(1 - \frac{\sqrt{2}}{2})\zeta(\frac{3}{2})(\frac{T}{T_F})^{3/2}$
High $T \gg T_F$	All q	$(\frac{T_F}{T})(1 - \frac{q^2 T_F}{6k_F^2 T})$	$\frac{T}{T_F}[\ln 4 + \frac{q^2}{24k_F^2}(\frac{T}{T_F})^2]$

assuming charged impurities as the dominant source of scattering and neglecting all other scattering sources (e.g., phonons). We find that the temperature dependent resistivity induced by the temperature-dependent screening is non-monotonic. It shows metallic behavior at low temperatures, but insulating behavior at high temperatures. The quadratic temperature-dependent correction to $\rho(T)$ at low temperatures is suppressed by level broadening effects which give rise to an effective linear temperature dependence of resistivity for $T \ll T_F$. Even though our Drude-Boltzmann transport theory explains both the high-density metallic behavior and the low-density insulating behavior as observed experimentally, we emphasize that the theory is strictly quantitatively valid only in the relatively high-density regime where our linear screening theory based on the homogeneous carrier density model is valid. In the low-density regime, near the Dirac point, it is well established that the graphene layer becomes spatially inhomogeneous with random charged impurity-induced electron-hole puddles dominating the carrier density profile.^{13,14} In this low-density inhomogeneous regime our linear screening theory, based on an average density approximation, is at best of qualitative validity. It is, therefore, not surprising that, although we obtain a reasonable quantitative agreement with experiment in the high-density regime away from the Dirac point where $\rho(T)$ manifests very weak metallic temperature dependence, our results are only in qualitative agreement with the experimental data in the low-density Dirac point regime where $\rho(T)$ shows an insulating temperature dependence.¹⁰ Loosely speaking, our screening theory is valid for $n > n_i$ so that the impurity-induced puddle formation is weak, but we believe that the qualitative behavior predicted by our theory has rather broad validity. Indeed, our theory provides a plausible qualitative explanation for the observed¹⁰ weakly metallic and strongly insulating behaviors of the temperature-dependent resistivity at high and low densities, respectively.

We conclude by pointing out that we have only considered in this work the contribution to the temperature-dependent graphene conductivity arising from screened Coulomb disorder, including both the explicit temperature dependence of the screening function and the implicit temperature dependence due to the thermal energy averaging in the Boltzmann theory. There are other scattering mechanisms contributing to the temperature dependence of carrier transport properties, most notably, phonon scattering which we have studied elsewhere.¹⁶ When the temperature dependence of the conductivity is weak, Matthiessen's rule should apply giving $\rho(T) = \rho_i(T) + \rho_{\text{ph}}(T)$, where $\rho_i(T)$, $\rho_{\text{ph}}(T)$ are, respectively, the graphene resistivity due to charged impurity scattering

TABLE III. Temperature-dependent conductivity $\sigma(T)$. Note $\sigma_0 \equiv \sigma(T=0)$.

Temperature (T)	2D system	Graphene
Low $T \ll T_F$	$\sigma(T)/\sigma_0 = 1 - O(T/T_F)$	$\sigma(T)/\sigma_0 = 1 - O[(T/T_F)^2]$
High $T \gg T_F$	$\sigma \sim O(T/T_F)$	$\sigma \sim O[(T/T_F)^2]$

and phonon scattering. Since $\rho_{\text{ph}}(T)$ is very strongly suppressed at low temperatures due to the well-known Bloch-Grüneisen behavior, it is reasonable to expect that $\rho(T)$ is dominated by $\rho_i(T)$, considered in this work, for $T \lesssim 50\text{--}100$ K depending on the carrier density. We note that $\rho_{\text{ph}}(T)$ due to phonon scattering is always monotonic in T , and therefore the insulating temperature dependence of $\rho(T)$ around the low-density Dirac point cannot arise from phonon scattering which would always produce a metallic $\rho_{\text{ph}}(T)$ increasing with increasing T (linearly at higher temperatures). It is, therefore, reasonable to conclude, as we do in this work, that the low- T insulating behavior of graphene $\rho(T)$ around the low-density Dirac point, as observed experimentally in Ref. 10, is a result of the high-temperature and low-density (i.e., $T/T_F \lesssim 0.5$) screened impurity-scattering phenomenon discussed in this work. More work will, however, be needed to understand this Dirac point insulating behavior quantitatively since the electron-hole puddle induced density inhomogeneity becomes important around the Dirac point.

ACKNOWLEDGMENT

This work is supported by U.S. ONR.

APPENDIX

We provide, for the sake of convenience, in this appendix the various formula comparing the basic electronic properties [e.g., Fermi wave vector, Thomas-Fermi (TF) wave vector, r_s parameter, density of states (DOS), Fermi energy, cyclotron frequency] in graphene and parabolic 2D systems; and (2) the analytic equations for the electronic polarizability and (3) the resistivity (arising from screened charged impurity scattering) in the low ($T \ll T_F$) and high ($T \gg T_F$) temperature limits for graphene and 2D systems. The results are given in terms of carrier density (n), Fermi velocity v_F (graphene) or effective mass m (2D systems), ground-state degeneracy g ($\equiv g_s g_v$ for spin and valley), background dielectric constant (κ), electron charge (e), and Planck constant (\hbar) in Tables I–III.

¹K. S. Novoselov, A. K. Geim, S. V. Morozov, D. Jiang, Y. Zhang, S. V. Dubonos, I. V. Grigorieva, and A. A. Firsov, *Science* **306**, 666 (2004).

²Y. Zhang, Y.-W. Tan, H. L. Stormer, and P. Kim, *Nature (London)* **438**, 201 (2005).

³Y.-W. Tan, Y. Zhang, K. Bolotin, Y. Zhao, S. Adam, E. H. Hwang, S. Das Sarma, H. L. Stormer, and P. Kim, *Phys. Rev. Lett.* **99**, 246803 (2007).

⁴J. H. Chen, C. Jang, S. Adam, M. S. Fuhrer, E. D. Williams, and M. Ishigami, *Nat. Phys.* **4**, 377 (2008).

- ⁵See, for example, the special issues of Solid State Commun. **143**, 1 (2007); and Eur. Phys. J. Spec. Top **148**, 1 (2007).
- ⁶K. I. Bolotin, K. J. Sikes, Z. Jiang, M. Klima, G. Fudenberg, J. Hone, P. Kim, and H. L. Stormer, Solid State Commun. **146**, 351 (2008).
- ⁷Y.-W. Tan, Y. Zhang, H. L. Stormer, and P. Kim, Eur. Phys. J. Spec. Top. **148**, 15 (2007).
- ⁸S. V. Morozov, K. S. Novoselov, M. I. Katsnelson, F. Schedin, D. C. Elias, J. A. Jaszczak, and A. K. Geim, Phys. Rev. Lett. **100**, 016602 (2008).
- ⁹J. H. Chen, C. Jang, S. Xiao, M. Ishigami, and M. S. Fuhrer, Nat. Nanotechnol. **3**, 206 (2008).
- ¹⁰K. I. Bolotin, K. J. Sikes, J. Hone, H. L. Stormer, and P. Kim, Phys. Rev. Lett. **101**, 096802 (2008).
- ¹¹T. Ando, J. Phys. Soc. Jpn. **75**, 074716 (2006).
- ¹²V. V. Cheianov and V. I. Fal'ko, Phys. Rev. Lett. **97**, 226801 (2006).
- ¹³E. H. Hwang, S. Adam, and S. Das Sarma, Phys. Rev. Lett. **98**, 186806 (2007).
- ¹⁴S. Adam, E. H. Hwang, V. M. Galitski, and S. Das Sarma, Proc. Natl. Acad. Sci. U.S.A. **104**, 18392 (2007); E. H. Hwang, S. Adam, and S. Das Sarma, Phys. Rev. B **76**, 195421 (2007).
- ¹⁵K. Nomura and A. H. MacDonald, Phys. Rev. Lett. **96**, 256602 (2006).
- ¹⁶E. H. Hwang and S. Das Sarma, Phys. Rev. B **77**, 115449 (2008).
- ¹⁷T. Stauber, N. M. R. Peres, and F. Guinea, Phys. Rev. B **76**, 205423 (2007).
- ¹⁸S. Fratini and F. Guinea, Phys. Rev. B **77**, 195415 (2008).
- ¹⁹F. T. Vasko and V. Ryzhii, Phys. Rev. B **76**, 233404 (2007).
- ²⁰E. Mariani and F. von Oppen, Phys. Rev. Lett. **100**, 076801 (2008).
- ²¹S. V. Kravchenko, W. E. Mason, G. E. Bowker, J. E. Furneaux, V. M. Pudalov, and M. DiIorio, Phys. Rev. B **50**, 8039 (1994); **51**, 7038 (1995).
- ²²S. Das Sarma and E. H. Hwang, Solid State Commun. **135**, 579 (2005); E. Abrahams, S. V. Kravchenko, and M. P. Sarachik, Rev. Mod. Phys. **73**, 251 (2001).
- ²³S. Das Sarma and E. H. Hwang, Phys. Rev. Lett. **83**, 164 (1999).
- ²⁴T. Ando, A. B. Fowler, and F. Stern, Rev. Mod. Phys. **54**, 437 (1982).
- ²⁵A. H. Castro Neto, F. Guinea, N. M. R. Peres, K. S. Novoselov, and A. K. Geim, Rev. Mod. Phys. **81**, 109 (2009).
- ²⁶E. H. Hwang and S. Das Sarma, Phys. Rev. B **77**, 195412 (2008).
- ²⁷E. H. Hwang and S. Das Sarma, Phys. Rev. B **75**, 205418 (2007); B. Wunsch, T. Stauber, F. Sols, and F. Guinea, New J. Phys. **8**, 318 (2006).
- ²⁸G. Zala, B. N. Narozhny, and I. L. Aleiner, Phys. Rev. B **64**, 214204 (2001).
- ²⁹S. Das Sarma and E. H. Hwang, Phys. Rev. B **68**, 195315 (2003).
- ³⁰S. Das Sarma and E. H. Hwang, Phys. Rev. B **69**, 195305 (2004).
- ³¹M. Y. Simmons, A. R. Hamilton, M. Pepper, E. H. Linfield, P. D. Rose, D. A. Ritchie, A. K. Savchenko, and T. G. Griffiths, Phys. Rev. Lett. **80**, 1292 (1998).
- ³²M. P. Lilly, J. L. Reno, J. A. Simmons, I. B. Spielman, J. P. Eisenstein, L. N. Pfeiffer, K. W. West, E. H. Hwang, and S. Das Sarma, Phys. Rev. Lett. **90**, 056806 (2003).
- ³³V. Senz, T. Ihn, T. Heinzl, K. Ensslin, G. Dehlinger, D. Grutzmacher, U. Gennser, E. H. Hwang, and S. Das Sarma, Physica E **13**, 723 (2002).
- ³⁴S. J. Papadakis and M. Shayegan, Phys. Rev. B **57**, R15068 (1998).
- ³⁵S. Das Sarma, Phys. Rev. B **33**, 5401 (1986).
- ³⁶T. Ando, J. Phys. Soc. Jpn. **51**, 3215 (1982); P. G. de Gennes, J. Phys. Radium **23**, 630 (1962); S. K. Lyo, J. Phys. C **21**, 3577 (1988).